Processes Influencing Rain-Field Growth and Decay after Tropical Cyclone Landfall in the United States

CORENE J. MATYAS

Department of Geography, University of Florida, Gainesville, Florida

(Manuscript received 21 June 2012, in final form 13 December 2012)

ABSTRACT

This study measured rain-field sizes for tropical cyclones (TCs) after U.S. landfall and related changes in size to the diurnal cycle and extratropical transition (ET). For 45 TC landfalls, the spatial properties of the rain fields were calculated through an analysis of radar reflectivity returns within a geographic information system. Variables representing the conditions of the atmosphere and storm attributes were examined at three times and as changes over two time periods to account for lags between condition onset and change in raining-area sizes. Mann–Whitney *U* tests illustrated which of these variables had significantly different median values when the total raining area or high-reflectivity regions increased or decreased in areal extent over two 12-h periods after landfall. Results indicate that the diurnal cycle influenced changes in rain-field size. Rain-field growth occurred during the late morning and early afternoon, which is between the times for peak areal extent of oceanic- and land-based precipitation in the tropics. The rain fields of TCs completing an ET within 74 h of landfall increased in areal extent during the first 12 h after landfall and decayed during the second 12-h period as they neared the completion of ET. The availability of moisture, which was not related to either the diurnal cycle or processes associated with ET, was also important to rain-field growth or decay. In addition, it was discovered that, for the United States, landfall times have shifted from a peak before midnight during 1950–96 to after midnight during 1995–2008.

1. Introduction

The rainfall that tropical cyclones (TCs) produce as they move over land can be beneficial to alleviate drought conditions (Maxwell et al. 2012). Extensive freshwater flooding can also occur, however, especially when the storm is slow moving (Konrad et al. 2002), the underlying terrain is sloped (Haggard et al. 1973), and/ or previous rains have saturated the ground (Sturdevant-Rees et al. 2001). More than one-half of the deaths in the United States that are related to TCs are a result of freshwater flooding (Rappaport 2000; Czajkowski et al. 2011). When TC rain fields increase in size after landfall, more locations receive rainfall and the overall duration of rainfall is longer for a given location. Both convective precipitation and stratiform precipitation occur within TCs (Jorgensen 1984; Yokoyama and Takayabu 2008), and, whether rainfall is moderate or heavy, a longer duration of rainfall increases the chances that flooding and associated damage and deaths can occur. A better understanding of the physical processes that are associated with TC rain-field growth and decay as these storms move over land is needed to improve rainfall forecasts.

In the tropics and midlatitudes during the warm season, the growth and decay of convective clouds is strongly associated with the diurnal cycle. Oceanic convection peaks in the morning between 0600 and 1000 LST, and researchers have postulated that day–night differences in radiative cooling that alter environmental lapse rates within and outside the storm environment may explain the timing of this peak (Gray and Jacobson 1977; Yang and Smith 2006; Kikuchi and Wang 2008). As TCs form over the ocean, their diurnal cycles of convection exhibit a morning peak coincident with other oceanic convection as observed by researchers examining cloud-top temperatures from satellite observations (Browner et al. 1977; Muramatsu 1983; Lajoie and Butterworth 1984; Steranka et al. 1984; Kossin 2002). It follows that the area covered by high rainfall rates would be larger after midnight than after noon. Rainfall observations from islands in the tropical oceans as well as satellite-based rainfall

Corresponding author address: Corene J. Matyas, 3141 Turlington Hall, Dept. of Geography, University of Florida, Gainesville, FL 32611.
E-mail: matyas@ufl.edu

DOI: 10.1175/JAMC-D-12-0153.1

estimations support this expectation (Frank 1977; Lajoie and Butterworth 1984; Jiang et al. 2011).

The timing of peak rainfall activity over landmasses differs from that over the ocean. Diurnal changes in air temperature are greater over the land surface than over the ocean as sensible heat flux plays a larger role relative to latent heat flux in the energy budget. Land-based convection peaks in the afternoon and early evening between 1600 and 1900 LST when upward sensible heat flux is maximized so that the lower troposphere is destabilized (Wallace 1975; Dai 2001; Yang and Smith 2006; Dai et al. 2007). Once fully over the land surface, TC rain fields may also be larger in the afternoon relative to the morning. Yet, during landfall TCs may spend several hours near the coast where the timing of peak rainfall activity can differ from that over land or ocean (Yang and Smith 2006). Muramatsu (1983) showed that, for two typhoons moving within 250 km of Okinawa, an afternoon peak in convective clouds developed around 1500 LST, which is slightly earlier than the peak identified for land-based convection but much later than that for oceanic convection. A larger sample of landfalling TCs must be analyzed to better determine how the diurnal cycle influences rain-field growth and decay for TCs over land.

Processes related to extratropical transition (ET) also affect rain-field growth or decay. During recurvature, interaction with midlatitude troughs can restructure a TC into an extratropical cyclone, causing both the wind and rain fields to expand (Rodgers et al. 1991; Jones et al. 2003). Hart and Evans (2001) found that nearly one-half of Atlantic Ocean basin TCs complete an ET and that most major cities north of 35°N in the eastern United States have received rainfall from one or more of these systems. The changes in environmental conditions during ET include increased baroclinicity, enhanced horizontal moisture gradients, high vertical wind shear, increased positive vertical vorticity and relative eddy momentum flux convergence, and faster steering flows (Atallah and Bosart 2003; Jones et al. 2003). Isentropic ascent of warm and moist tropical air ahead of the storm often causes rain fields to expand in a delta-shaped area ahead of the storm center (Harr and Elsberry 2000; Klein et al. 2000; Ritchie and Elsberry 2001). Meanwhile, the advection of relatively drier and cooler air around the south side of the storm reduces rainfall in that area. According to Klein et al. (2000), the timeline for ET spans 74 h: transformation averages 46 h, with another 28 h required for reintensification.

A limitation of many previous satellite-based studies of diurnal peaks in rainfall is the selection of a temperature threshold for analysis of cloud-top temperatures as the timing of peak areal coverage is dependent upon this threshold (Muramatsu 1983; Lajoie and Butterworth 1984). Ground-based radar reflectivity data provide a spatially accurate representation of the areal coverage of TC rain fields over land areas without this limitation. This study employed a geographic information system (GIS) to measure the areal extent of radar reflectivity returns associated with 45 TC landfalls in the United States. The main hypothesis was that the diurnal cycle will cause growth to occur later in the morning relative to oceanic convection but earlier in the afternoon than is seen for land-based convection. Thus, making landfall after midnight should result in rainfall regions of TCs that increase in areal coverage over the next 12 h, followed by a decrease in areal coverage for 12–24 h after landfall, whereas the opposite should occur for landfall after noon. The second hypothesis was that processes associated with ET also influence changes in rain-field size. TCs classified as ET within 74 h of landfall should exhibit this pattern as this is the timeline for ET completion identified by Klein et al. (2000). To test these hypotheses, cases were grouped according to whether the total raining area or high-reflectivity regions increased or decreased in areal extent over 12-h periods. Mann–Whitney *U* tests (Mann and Whitney 1947) were employed to discover whether variables associated with the diurnal cycle such as time of day and relative humidity, and/or variables linked to conditions associated with ET such as fast motion to the north and east have statistically significant differences in median values for cases in which rain fields grow versus those in which they decay.

2. Data and methods

a. Radar analysis

The number of storms examined was determined by the availability of the radar reflectivity data utilized to delineate the spatial extent of the rain fields. Data from the Weather Surveillance Radar—1988 Doppler (WSR-88D) network are available in each degree of the 360° sweep every 1 km outward from the radar site with an outer distance limit of 230 km (OFCM 2006). During 1995–2008, there were 45 cases for which 1) radar reflectivity data were available and 2) the rain fields of the TCs remained within range of the WSR-88D network for a minimum of 24 h after landfall. Level-III base reflectivity product data were utilized to retain a large sample size, and these data were obtained online from the National Climatic Data Center's archive (http://www.ncdc.noaa.gov/nexradinv/). This product is generated after the removal of ground clutter and consists of reflectivity values from the lowest scan (0.5° tilt) that are

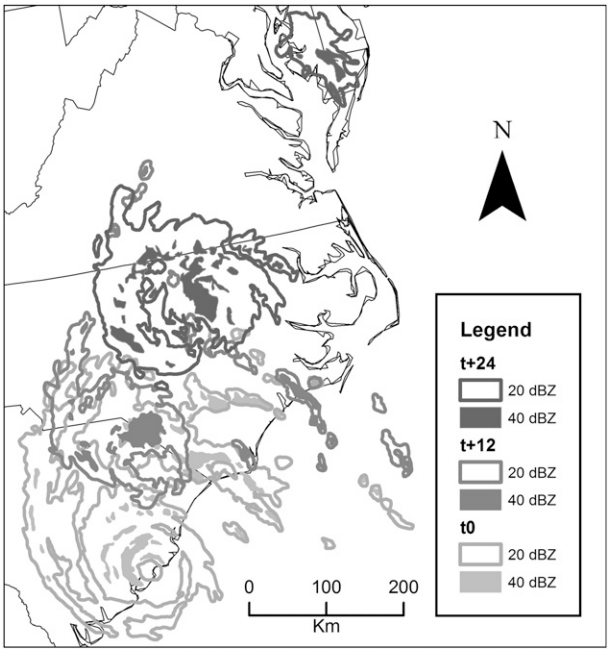

FIG. 1. Areas composed of radar reflectivity values of 20 dBZ and higher and 40 dBZ and higher for Hurricane Gaston (2004) at the three analysis times considered in the current study (t_0, t_{+12}, and t_{+24}).

rounded to the nearest 5 dBZ (OFCM 2006). Level-II data that include values from all scan elevations are not available for six radars after 2001; therefore, use of these data would have significantly decreased the number of cases analyzed.

Base reflectivity data collected during the scan nearest the time of landfall t_0, 12 h after landfall t_{+12}, and 24 h after landfall t_{+24} at each radar were imported into a GIS. After the data were transformed into an equal-area projection, a mosaic was created for each time step. The highest value was retained in cases in which data from adjoining radars overlapped. The reflectivity values were then contoured in 5-dBZ increments, and a 10-km smoothing filter was applied. After the conversion of contours into polygons (Fig. 1), their areal extent was calculated. In the event that residual ground clutter remained, polygons with areal extents of less than 25 km^2 were removed from the analysis. Although the author then visually inspected each case as an additional measure of quality control, it is possible that ground clutter from anomalous propagation may still be embedded within precipitation, which could extend the echo areal coverage. From the work of previous TC researchers, the total raining area was defined as the area occupied by reflectivity values of greater than or equal to 20 dBZ (Jorgensen 1984; Barnes et al. 1991; Matyas 2007). This area is composed of low, moderate, and high rain rates

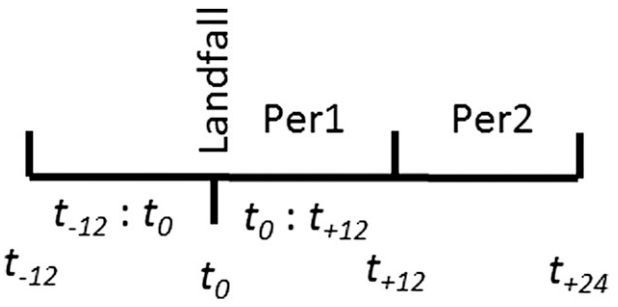

FIG. 2. Timeline for analysis of atmospheric conditions and measurements of rain-field area.

formed through stratiform and convective processes (Jorgensen 1984; Houze 1993; Steiner et al. 1995). To examine the high-rain-rate regions most likely to have formed through convective processes, the areas occupied by reflectivity values greater than or equal to 40 dBZ were also extracted for analysis. This threshold was selected based on previous research that classified convective regions of clouds (Parrish et al. 1982; Jorgensen 1984; Tokay and Short 1996; Biggerstaff and Listemaa 2000). The area occupied by reflectivity values at the time of landfall was subtracted from that at t_{+12} to calculate the change in area over the first 12-h period following landfall (Per1). Areas at t_{+12} were subtracted from those at t_{+24} to calculate the change in area over the second 12-h period following landfall (Per2) (Fig. 2).

b. Characterization of storm attributes and environmental conditions

All data pertaining to storm location and attributes as well as environmental conditions were interpolated linearly to the time of landfall. The time of landfall, coordinates of the circulation center, and intensity were obtained from the Hurricane Season Tropical Cyclone Reports available online from the National Hurricane Center (NHC; http://www.nhc.noaa.gov; Rappaport et al. 2009). These reports were also utilized to determine whether a TC became extratropical and the time that it did so if applicable. The Hurricane Database (HURDAT; Jarvinen et al. 1984) provided the coordinates of the circulation center, storm heading, forward velocity, and intensity at 0000, 0600, 1200, and 1800 UTC. Storm motion was subdivided into northward and eastward components.

Atmospheric conditions were characterized through data obtained from the Statistical Hurricane Intensity Scheme (SHIPS) database (DeMaria and Kaplan 1994; DeMaria et al. 2005). The SHIPS variables are derived from the National Centers for Environmental Prediction (NCEP) Global Forecast System model analyses, and most variables are calculated for an annular region that is

TABLE 1. Name, abbreviation, unit of measure, and source for variables that were used in the study. Variables from HURDAT, SHIPS, and NARR have five variations (three instantaneous times and two changes over time) that were subjected to Mann–Whitney *U* tests.

Variable	Abbreviation	Units	Source
Latitude	Lat	°N	HURDAT
Longitude	Lon	°W	HURDAT
Motion north	MotN	m s^{-1}	HURDAT
Motion east	MotE	m s^{-1}	HURDAT
Velocity of max sustained winds	$\mathbf{V}_{max}$	m s^{-1}	HURDAT
Min central pressure	MCP	hPa	HURDAT
Southerly vertical wind shear	ShrS	m s^{-1}	SHIPS
Westerly vertical wind shear	ShrW	m s^{-1}	SHIPS
Air temperature at 200 hPa	T200	°C	SHIPS
Zonal winds at 200 hPa	U200	m s^{-1}	SHIPS
Divergence 200 hPa	D200	$s^{-1} \times 10^7$	SHIPS
Relative humidity high (500–300 hPa)	RhHi	%	SHIPS
Relative humidity middle (700–500 hPa)	RhMd	%	SHIPS
Relative humidity low (850–700 hPa)	RhLo	%	SHIPS
Vorticity at 850 hPa	Z850	$s^{-1} \times 10^7$	SHIPS
Relative eddy momentum flux convergence	REFC	m s^{-1} day^{-1}	SHIPS
Air temperature at 2 m	T2m	°C	NARR
Relative humidity at 2 m	Rh2m	%	NARR
Distance inland 12 h after landfall	Din12	km	GIS analysis
Distance inland 24 h after landfall	Din24	km	GIS analysis
Sine of landfall time minus value*	e.g., SinLT-90	Dimensionless	NHC report

* Eight values were utilized: 0, 45, 90, 135, 180, 225, 270, and 315.

200–800 km from the circulation center. Data are available at the standard synoptic times. Within the SHIPS dataset, deep-layer vertical wind shear is calculated over 850–200 hPa. For the current study, this vector was subdivided into south-to-north and west-to-east components. Vorticity at 850 hPa and 200-hPa divergence are derived for a radius of 0–1000 km about the circulation center, and 200-hPa relative eddy momentum flux convergence (REFC) is averaged over 100–600 km. Previous research (e.g., Jones et al. 2003) suggests that many of the 10 variables derived from the SHIPS dataset (Table 1) should exhibit differences for TCs that become extratropical within 74 h of landfall as compared with those that do not.

Solar heating during the day and loss of longwave radiation during the night drive the diurnal cycle of air temperature near Earth's surface, and changes in relative humidity (RH) are affected by air temperature as well as soil moisture and precipitation (Dai 2001). Thus, the strongest evidence that the diurnal cycle may influence changes in the sizes of rain fields while TCs move over land should be found through an analysis of near-surface temperature and RH values. To examine these variables every 3 h, values were obtained from NCEP's North American Regional Reanalysis (NARR) database (Mesinger et al. 2006). Air temperature and RH data at 2 m above ground level were converted into ''shapefile'' format and entered into a GIS. Buffers of 200 and 800 km from the circulation center at each analysis time were used to select only the data points inside this distance range. The average value of data points over this region was then utilized in the analysis for compatibility with the other SHIPS variables.

The values for all variables mentioned above were analyzed at three different times relative to landfall. Previous research has shown that a time lag of 12–24 h exists between the onset of environmental conditions and resulting changes in TC structure (e.g., Frank and Ritchie 1999; Kimball 2008; Matyas 2010). To account for this lag effect, environment conditions were analyzed at t_{-12}, t_0, and t_{+12}, which coincide with 24, 12, and 0 h prior to the end of Per1 and 36, 24, and 12 h prior to the end of Per2 (Fig. 2). In addition, the changes in the environmental conditions over each 12-h period were calculated as these values may be more representative of the diurnal cycle or progression of conditions associated with ET than the actual value of the variable at any one time. For example, a 12-h increase in RH and decrease in air temperature indicate that the midpoint of the period occurs near dawn, whereas increasing storm forward velocity coincides with the progression of an ET. Thus, each environmental condition derived from HURDAT, SHIPS, and NARR was explored at three instantaneous times (t_{-12}, t_0, and t_{+12}) and over two periods (t_{-12}:t_0 and t_0:t_{+12}), yielding 90 total variables (Table 1).

As a TC moves inland, its center of circulation becomes farther removed from the warm ocean waters that supply the primary source of latent heat to sustain the storm (e.g., Tuleya 1994). It follows that, in general, the

greater the distance between the nearest point along the coastline and the circulation center of a TC is, the less is the potential for rainfall enhancement as the availability of low-level moisture is reduced. Remaining near the coastline may allow rain fields to grow regardless of the time of day or whether the storm is undergoing ET. Within a GIS, the U.S. coastline from Brownsville, Texas, to Eastport, Maine, was converted into a line feature and the ''Near'' function calculated the distance between the position of the circulation center at 12 and 24 h after landfall and the nearest point along the line representing the coast.

The inclusion of the local time of each TC's landfall in the statistical analysis is important because it reveals which landfall times are most associated with postlandfall growth or decay. For example, if the rain fields of landfalling TCs exhibit a diurnal cycle similar to that of ocean-based convection in which peak activity occurs at 0600–1000 LST, then a rain-field size that is larger at t_{+12} than at landfall should occur for landfall times ranging from 1800 to 2200 LST. After the conversion of landfall time from UTC to LST, each hour was multiplied by 15 to extend the range of values to 360. So that landfall times occurring every 3 h were represented in the analysis, a value of 45 was subtracted from each converted time. After converting these values into radians, the sine of all eight values was calculated. As a result, the sine of the landfall time minus 180 (SinLT-180) produces a value of 1.0 for the landfall time of 1800 LST and −1.0 for the time of 0600 LST. If the diurnal cycle for landfalling TCs was coincident with that of oceanic-based convection, then rain-field growth would occur during the 12-h periods of 1800–0600 and 2100–0900 LST, and these periods would be indicated by values near 1.0 for variables SinLT-180 and SinLT-225.

c. *Statistical analyses*

This study employs nonparametric Mann–Whitney *U* tests (MWU; Mann and Whitney 1947) to relate differences in environmental conditions to rain-field growth or decay. This test compares the medians of variables when cases are divided into two independent groups, with a null hypothesis that data from the two groups originate from the same population. This test was utilized because it is more robust for skewed data than is an independent samples *t* test and is less likely to yield false results when group sizes are small and/or not equal (Wilks 1995). For each variable, values are ranked regardless of group membership. The test statistic then compares the sum of the ranks from the first group with that of the second. If the samples are drawn from the same population, the summed total of ranks for each group should be similar. In the current study, the null hypothesis was rejected when *p* values were less than a significance level of 0.05, which is a commonly used level according to Wilks (1995). Although the variables tested are not independent, the performance of 100 individual MWU tests within each set as described below does increase the possibility of incorrectly rejecting the null hypothesis when the experiment-wise error rate is considered. However, the technique is valid given that the acceptance of the two main hypotheses of the study does not rely solely on the results of any one test; a number of variables are representative of the diurnal cycle and ET. All *p* values meeting the 0.05 threshold are reported so that results can also be scrutinized more stringently if desired.

For each MWU test, cases were grouped according to whether rainfall areas increased or decreased during a 12-h period. Two different 12-h periods and two radar reflectivity thresholds to calculate the rain-field area were analyzed, yielding four sets of MWU tests in which all 100 variables (discussed in section 2b) were grouped according to rain-field growth or decay. Set 1 examined rain-field growth or decay for total raining area during Per1, and set 2 compared growth and decay for high-reflectivity regions during Per1. In sets 3 and 4, cases were grouped according to rain-field growth or decay during Per2, with set 3 (4) focusing on total raining area (high-reflectivity regions). Variables for which the null hypothesis is rejected identify the conditions associated with rain-field growth or decay during each period. The influence of the diurnal cycle may be indicated by variables such as 12-h changes in near-surface air temperature and RH along with the variations in sine of the landfall time. In other words, if the mean rank of the 12-h change in air temperature or RH for rain-field growth cases differs from the mean rank of the 12-h change for rain-field decay cases, then a diurnal effect may be occurring. In 20 cases, TCs made the transition to extratropical cyclones within 74 h of landfall. If the null hypothesis is rejected for variables characterizing storm motion, vorticity, REFC, and vertical wind shear, it indicates that processes associated with ET influence rain-field growth and decay. Note that landfall occurred at various times of day for TCs that became extratropical within 74 h of landfall.

3. Results

a. *Rain-field sizes and statistics*

At the time of landfall, the median rain field had an area of 109 263 km^2 and the median value for high-reflectivity regions was 10 473 km^2 (Fig. 3). Hurricane Floyd (1999) was an outlier (not visible in Fig. 3), having the largest extent of both measures of rainfall area. TCs

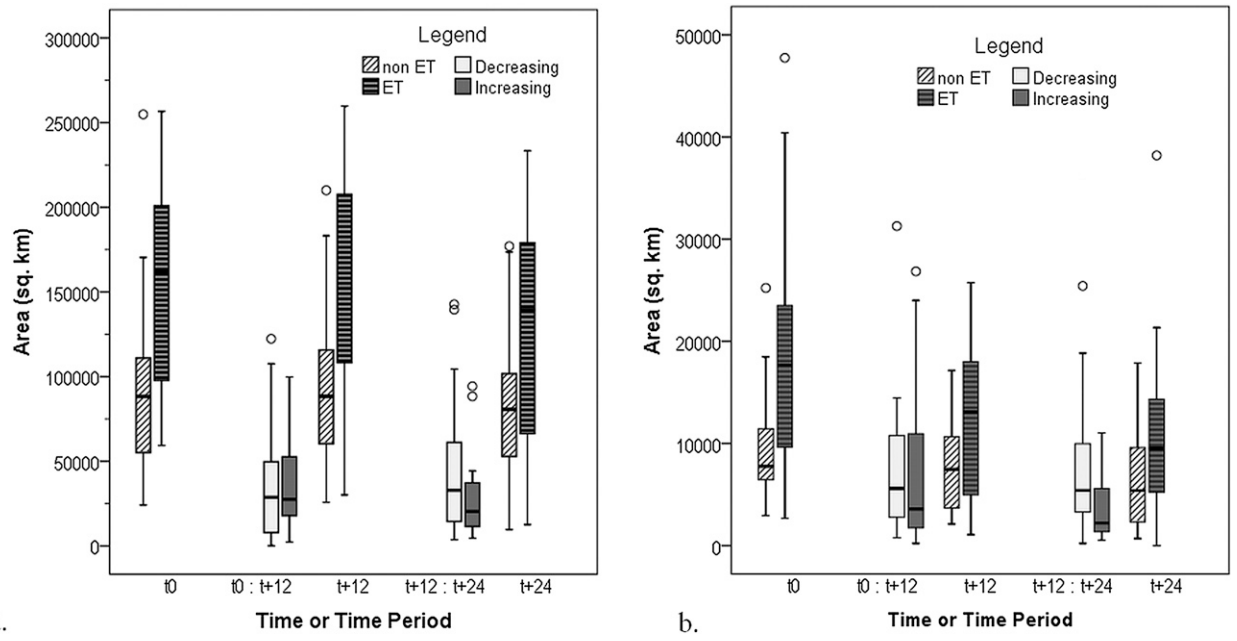

FIG. 3. Areal coverage of rain fields for TCs that became extratropical (labeled ET) within 74 h of landfall as compared with those that did not (''non ET'') at t_0, t_{+12}, and t_{+24} and the change in area for TCs that decayed (decreasing) and grew (increasing) during t_0:t_{+12} and t_{+12}:t_{+24} for (a) total raining area and (b) high-reflectivity regions. Hurricane Floyd (1999) was an outlier, with values that would appear off the top of each panel.

such as Floyd that became extratropical within 74 h had the largest rain fields (Fig. 3). Nine of 13 TCs with total raining areas that were larger than 150 000 km^2 and 11 of 16 TCs with high-reflectivity regions that spanned more than 15 000 km^2 completed an ET within 60 h of landfall. Spearman's rank correlation coefficients (not shown) demonstrate that the time of landfall was not significantly correlated with rain-field size. Yet, the diurnal cycle may be influencing the timing of rain-field growth and decay given that over Per1 larger rain fields decreased while smaller rain fields increased in areal coverage. As a result, the mean and median areas were similar to the values at landfall. During Per1, 23 (21) of 45 cases experienced increases in total raining area (high-reflectivity regions). Rain-field (high reflectivity) growth occurred for 14 (16) of 45 cases during Per2. Although by t_{+24} median rainfall areas had decreased from that at landfall, 19 (12) TCs increased in areal coverage for total raining area (high-reflectivity regions) during this period, with a mean increase of 27 734 km^2 (4228 km^2).

b. *Results of the Mann–Whitney* U *tests*

The outcomes of the four sets of MWU tests support the hypotheses that the diurnal cycle and ET affect rain-field growth and decay. There were 51 variables with p values of less than or equal to 0.05 (Tables 2–5). Of these, 20 were unique to one set and two variations of the sine of landfall time were significant in all four sets of tests, indicating that rain-field growth occurred when either Per1 or Per2 began near 0000 and 0300 LST. The statistically significant variables are broadly categorized as relating to 1) the diurnal cycle, 2) ET, and 3) the availability of moisture. At least one variable from each category appeared in each of the four sets, suggesting that all three processes influence rain-field growth and decay after landfall. The results also demonstrate the importance of including both instantaneous and change-in variables as well as 12- and 24-h time lags between condition onset and rain-field response. A more stringent p level of 0.025 (0.01) yields 21 (9) significant variables across the four sets of tests.

1) RAIN-FIELD GROWTH AND DECAY AND THE DIURNAL CYCLE

TCs making landfall near midnight and 0300 LST tended to grow during Per1 and decay during Per2, whereas the opposite was true for landfalls occurring near noon and 1500 LST (Fig. 4). Statistical evidence supporting this pattern was found through the time-related variables and near-surface temperature and RH values as hypothesized. Cases in which landfall occurred closer to midnight (value of SinLT-270 close to 1.0) or 0300 LST (value of SinLT-315 close to 1.0) were associated with growth during Per1 (Tables 2 and 3) and decay during Per2 (Tables 4 and 5). Landfalls occurring

TABLE 2. Results of Mann–Whitney U tests for rain-field growth vs decay for total raining area during Per1. For meaning of the abbreviated variable names see Table 1.

Variable	Time	Median value grow	Median value decay	U	Significance	Association
Din12	t_{+12}	66.22	144.10	134	0.007	Moisture
SinLT-270*	t_0	0.71	−0.26	367.5	0.009	Diurnal
RhMd	t_{-12}:t_0	2.00	−1.25	364	0.011	Moisture
SinLT-315**	t_0	0.71	−0.26	359	0.016	Diurnal
MotE	t_{+12}	0.28	−2.06	350	0.026	ET
Z850	t_{-12}:t_0	10.25	−5.21	349	0.027	ET
RhLo	t_{-12}:t_0	2.30	−0.10	346.5	0.031	Moisture
Lon	t_0:t_{+12}	0.50	−0.70	345.5	0.033	ET
RhHi	t_{-12}:t_0	1.00	−1.65	340	0.045	Moisture
MotE	t_{-12}:t_0	0.78	0.14	338	0.050	ET
REFC	t_{-12}:t_0	5.00	−0.38	338	0.050	ET

* High positive values indicate landfall time close to 0000 LST.
** High positive values indicate landfall time close to 0300 LST.

approximately 12 h offset from these times (values of SinLT-270 and SinLT-315 close to −1.0) experienced decay at first followed by growth during Per2. For both analysis periods, rain-field growth was associated with decreasing air temperatures and increasing RH values near the surface during the previous 12 h, indicating that this preceding period was during the night. During Per2, growth was associated with cases having lower RH values at the time of landfall (which occurred during the day) and values decreasing prior to and increasing after landfall. Correspondingly, near-surface temperatures increased prior to landfall and decreased after landfall for TCs whose rain fields grew during Per2. Overall, growth tended to occur during the late-morning and early-afternoon hours as areal coverage was greater at 1200 and 1500 LST than it was at 0000 and 0300 LST.

These times for rain-field growth occur between the times reported by previous researchers for oceanic and land-based convection. Because most oceanic convection peaks between 0600 and 1000 LST (Gray and Jacobson 1977; Yang and Smith 2006; Kikuchi and Wang 2008), landfalling TCs following this pattern would have had values near 1.0 for variables SinLT-180 and SinLT-225, indicating landfall at 1800 or 2100 LST and rain-field growth over the next 12 h. This scenario did not occur. Afternoon peaks in rainfall over land correspond to times of 1600–1900 LST (Wallace 1975; Dai 2001; Dai et al. 2007). TCs making landfall near 0600 LST did not tend to have larger raining areas 12 h later as the analysis of variable SinLT-0 did not produce statistically significant results in the MWU tests. One explanation for these findings is that TCs are making the transition from the diurnal cycle of an ocean-based storm to that of a land-based storm during landfall. As TCs advect moisture-laden tropical air masses over the land surface during the morning hours, it is possible that instability is enhanced so that convection develops earlier in the day than when the normal continental air mass is in place. Knowledge

TABLE 3. As in Table 2, but for high-reflectivity regions during Per1.

Variable	Time	Median value grow	Median value decay	U	Significance	Association
Din12	t_{+12}	45.64	145.75	109	0.001	Moisture
ShrS	t_{+12}	−1.34	1.92	110	0.002	ET
REFC	t_{-12}	5.33	8.58	136	0.008	ET
SinLT-270*	t_0	0.71	−0.26	358.5	0.015	Diurnal
Rh2m	t_{-12}:t_0	7.04	−2.31	351	0.024	Diurnal
SinLT-315**	t_0	0.71	−0.26	349.5	0.026	Diurnal
RhMd	t_{-12}:t_0	2.00	−0.65	345.5	0.033	Moisture
T2m	t_{-12}:t_0	−2.74	0.06	160	0.036	Diurnal
RhHi	t_{-12}:t_0	0.80	−2.15	341.5	0.042	Moisture
Lon	t_{+12}	−83.50	−88.74	340	0.045	ET
Rh2m	t_0	82.77	78.02	340	0.045	Diurnal
Lon	t_{-12}	−83.30	−88.58	339.5	0.047	ET
Lon	t_0	−83.65	−88.73	338	0.050	ET

* High positive values indicate landfall time close to 0000 LST.
** High positive values indicate landfall time close to 0300 LST.

TABLE 4. As in Table 2, but for total raining area during Per2.

Variable	Time	Median value grow	Median value decay	*U*	Significance	Association
Rh2m	t_0	77.19	82.16	107	0.007	Diurnal
SinLT-315*	t_0	0.71	−0.44	119	0.016	Diurnal
RhLo	t_0:t_{+12}	3.45	−0.30	315.5	0.017	Moisture
T2m	t_{-12}:t_0	0.19	−2.71	313	0.019	Diurnal
Rh2m	t_{-12}:t_0	−2.86	7.04	129	0.031	Diurnal
RhMd	t_0:t_{+12}	1.90	−1.30	307	0.033	Moisture
SinLT-270**	t_0	0.61	−0.79	132	0.037	Diurnal
Rh2m	t_0:t_{+12}	6.77	−5.89	302	0.037	Diurnal
Lat	t_0:t_{+12}	1.39	1.73	135	0.044	ET
T2m	t_0:t_{+12}	−2.41	0.81	138	0.050	Diurnal

* High positive values indicate landfall time close to 0300 LST.
** High positive values indicate landfall time close to 0000 LST.

that rainfall may commence earlier in the day than expected for a location allows weather forecasters to alert the public as preparations are made for the arrival of TC conditions.

The current study is believed to be the first to analyze radar reflectivity returns for a large sample of landfalling TCs in the United States and to associate rain-field growth and decay with the diurnal cycle. Jiang et al. (2011) provided the first documentation of diurnal variations of global TC rainfall using data from the Tropical Rainfall Measuring Mission (TRMM) satellite. The TRMM analysis showed that volumetric rainfall from TCs over land peaked at 0100–0730 LST and 1630–1930 LST. However, Jiang et al. (2011) examined global TC rainfall variations. Their Fig. 12 shows little diurnal variation for Atlantic-basin storms as compared with the other TC basins. Atmospheric conditions do vary climatologically among the different TC basins. For example, Vincent and Fink (2001) discuss differences in the precipitable water content for the western and eastern Pacific TC basins. Thus, it is possible that the timing of the peak overland rainfall from Atlantic-basin TCs differs from that observed in other basins where TC rain rates can be higher. Also, studies have shown that the shape of the coastline as well as topography of the land surface can alter storm structure. The unique features of the U.S. coastline may contribute to a peak in rainfall that differs in timing from other landfall locations (e.g., Rogers and Davis 1993; Cubukcu et al. 2000; Liu et al. 2007; Kimball 2008; Au-Yeung and Chan 2010).

2) CONDITIONS RELATED TO EXTRATROPICAL TRANSITION

Of the 45 cases examined, 20 became extratropical within 74 h of landfall (Fig. 4). This study finds that ET contributes to overall rain-field growth early in the process and decay as the process nears completion while

TABLE 5. As in Table 2, but for high-reflectivity regions during Per2.

Variable	Time	Median value grow	Median value decay	*U*	Significance	Association
Lon	t_0:t_{+12}	−1.12	0.62	103.5	0.002	ET
REFC	t_{-12}:t_0	−2.46	3.50	109	0.004	ET
Lon	t_{-12}:t_0	−1.16	0.23	113.5	0.005	ET
MotE	t_{+12}	−2.63	0.94	128.5	0.014	ET
T2m	t_{-12}:t_0	0.36	−2.71	336	0.014	Diurnal
Rh2m	t_0	76.48	82.03	129	0.015	Diurnal
Lat	t_0:t_{+12}	1.22	2.13	131.5	0.017	ET
T2m	t_0	27.81	26.15	330	0.020	Diurnal
MotN	t_{-12}:t_0	−0.08	1.63	141	0.031	ET
U200	t_{-12}:t_0	−1.25	4.48	141	0.031	ET
MotE	t_0	−1.93	0.68	145	0.039	ET
T2m	t_0:t_{+12}	−1.73	0.41	145	0.039	Diurnal
SinLT-315*	t_0	0.71	−0.44	146.5	0.042	Diurnal
Rh2m	t_{-12}:t_0	−1.36	6.97	148	0.046	Diurnal
RhMd	t_0:t_{+12}	0.68	−1.65	318.5	0.047	Moisture
Rh2m	t_0:t_{+12}	6.41	−4.98	315	0.049	Diurnal
SinLT-270**	t_0	0.71	−0.13	150.5	0.050	Diurnal

* High positive values indicate landfall time close to 0300 LST.
** High positive values indicate landfall time close to 0000 LST.

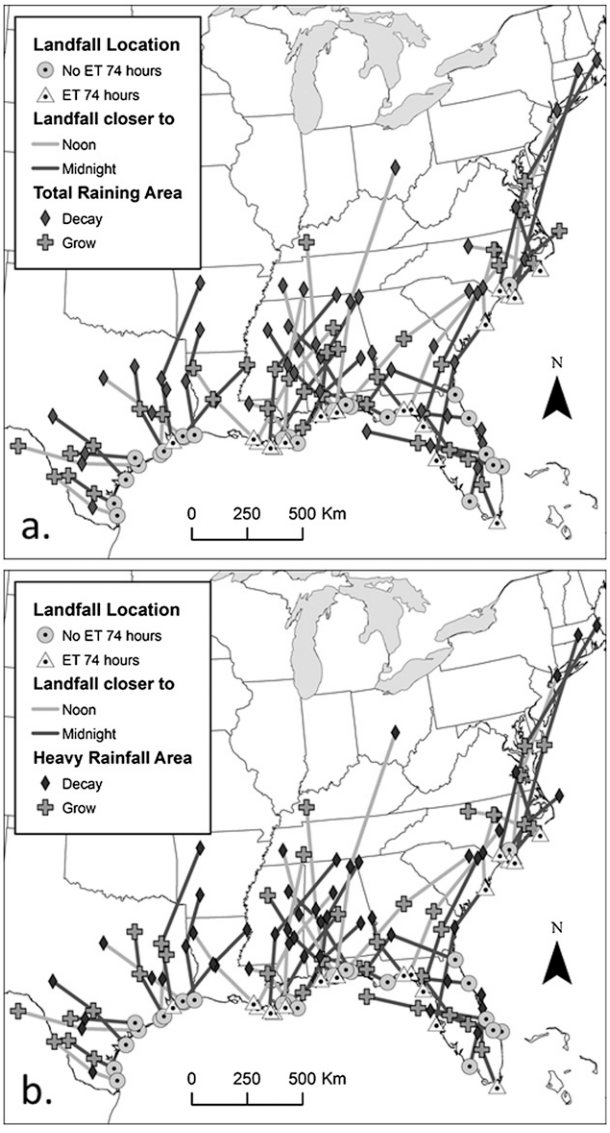

FIG. 4. Tracks of the 45 TCs, indicating whether landfall occurred closer to noon or midnight, whether ET occurred within 74 h of landfall, and whether rain fields grew or decayed during Per1 and Per2 for (a) total raining area and (b) high-reflectivity regions.

high-reflectivity regions mainly decayed. During Per1, ET storms exhibiting growth of the total raining area moved faster to the east while positive vorticity and REFC increased (Table 2). This net growth corresponds to descriptions of the development of the delta-shaped rain shield that occurs ahead of TCs in the early stages of ET (Harr and Elsberry 2000; Klein et al. 2000; Ritchie and Elsberry 2001). The tropical air mass that is advected over the cooler and drier air mass ahead of the storm center creates a stable environment that favors stratiform rather than convective processes. This explains why high-reflectivity regions decayed for ET cases. Higher values of vertical wind shear and REFC as well as longitudes located farther to the east as compared with cases in which high-reflectivity regions grew support the finding that ET contributes to this decrease in high-reflectivity regions (Table 3). For the five ET cases featuring growth in high-reflectivity regions during Per1, landfall occurred near midnight LST, indicating that the diurnal cycle may have contributed to the growth of these regions in the late-morning hours. Thus, it is likely that the diurnal cycle affects convective rainfall growth and decay even when ET is occurring.

The advection of relatively cool and dry air around the western and then southern side of the TC decreases rainfall production during step 3 of the transformation stage of ET (Klein et al. 2000). The current study supports this previous work. Save for one case in which the diurnal cycle may have contributed to rain-field growth, all TCs completing ET within 30 h of landfall experienced decay in both rainfall areas during Per2. TCs moving farther to the north decayed in total raining area as compared with those that remained south (Table 4). For high-reflectivity regions, decay during Per2 was associated with ET as fast northward and eastward motion and fast westerly winds at 200 hPa with increased REFC before landfall (Table 5).

3) IMPORTANCE OF MOISTURE FOR GROWTH AND DECAY

During Per1, one of the most significant differences between cases experiencing rain-field growth or decay was the distance inland traveled by storms in each group. TCs remaining closer to the coastline grew while those located more than twice as far inland decayed (Tables 2 and 3). Previous research has shown that TCs remaining closer to the coastline can have larger rain fields that produce more rainfall because remaining near the coastline allows TCs to draw in low-level moisture from the ocean to increase rainfall production (Lonfat et al. 2007; Matyas 2007; Medlin et al. 2007). Yet, the distance traveled inland by t_{+24} was not significant for Per2, and Spearman's rank correlation coefficients calculated between variable Din24 and the actual areal coverage rainfall (not shown) did not produce statistically significant results. Previous research has shown that rainfall production can still increase for TCs located more than 500 km inland if a low-level jet advects moisture into the storm, soil moisture is high enough to supply more latent heat flux than is experienced over dry land, or orographic enhancement of rainfall occurs (Haggard et al. 1973; Bluestein and Hazen 1989; Tuleya 1994; Emanuel et al. 2008; Arndt et al. 2009; Kellner et al. 2012). Thus, tracking far inland does not necessarily mean that rain fields will decrease in areal coverage.

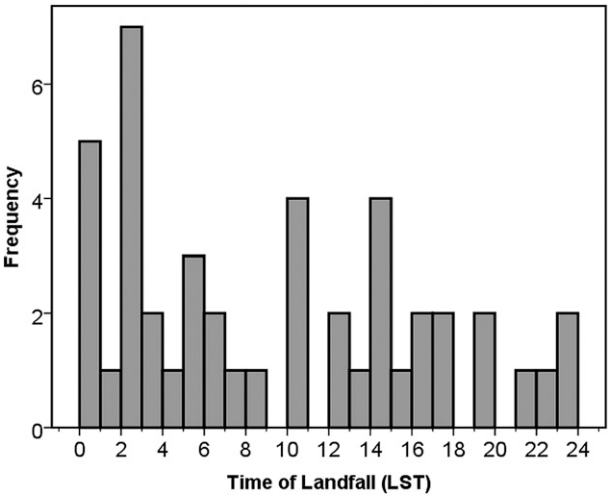

FIG. 5. Frequency of landfall times for the 45 cases in the study.

Moisture above the boundary layer is also important as rain-field growth was associated with increasing RH values in the low, middle, or high troposphere during the previous 12 h (Tables 2–5). A relatively moist surrounding environment is key to increased TC rainfall production (Jiang et al. 2008; Hill and Lackmann 2009; Matyas 2010). The advection of dry air into the system enhances evaporation, which leads to a decrease in rainfall production (Chan et al. 2004; Kimball 2008). Additional MWU tests performed with these RH variables and cases grouped according to whether or not ET occurred within 74 h of landfall and whether landfall occurred during the day or night indicated that changes in RH above the boundary layer were not strongly associated with either the diurnal cycle or ET.

c. Diurnal variations in landfall times

An examination of the distribution of landfall times for TCs in the current study yields an interesting result when compared with a previous study. One-third of the landfalls in the current study occurred between 0000 and 0300 LST (Fig. 5). In contrast, Konrad (2001) found that for 1950–96 nearly one-half of TCs landfalling along the Gulf of Mexico and Atlantic coastlines of the United States did so between 1700 and 0000 LST whereas only four landfalls occurred between 0100 and 0300 LST. After binning the landfall times in the current study according to the time groups listed in Table 1of Konrad (2001), a chi-square test showed statistically significant differences between the observed and expected distributions of cases among the landfall-time categories for the two datasets ($\chi^2 = 10.912; p = 0.012$). To rule out the possibility that the current study's sample was not representative of all landfalls during 1995–2008, an additional chi-square test revealed that the distribution of the current study very strongly resembles the distribution of the entire population ($\chi^2 = 0.836; p = 0.858$). Thus, it appears that a shift in landfall times has taken place from 1950–96, when the majority of landfalls occurred in the evening hours prior to midnight, to 1995–2008, when many occurred at or just after midnight.

A shift in the majority of TC landfalls from before to after midnight has important implications for the receipt of hurricane warning messages by the public. Prior to 2010, the NHC issued hurricane warnings when hurricane conditions were expected for the area within 24 h (Sheets 1990; Rappaport et al. 2009). With peak landfalls occurring between 1700 and 0000 LST, these warnings would likely have reached people during the late afternoon and evening hours, giving them adequate time to make preparations. During the more recent period when landfalls peaked at and after midnight, these warnings were more likely to have been issued after people had retired for the evening. Upon awakening the next morning, they may then have had less than 18 h to complete preparations for the arrival of hurricane-force winds. In 2010, the NHC changed its lead time so that hurricane warnings are now issued 36 h in advance of the anticipated onset of tropical storm–force winds (NHC 2012). The new longer lead times reduce the problems with TCs making landfall after midnight, which has become more common in recent years (Fig. 5).

4. Conclusions and future research

In this study, the areal coverage of TC rain fields was examined after U.S. landfall through a GIS-based spatial analysis of radar reflectivity returns. The growth and decay of the total raining area and high-reflectivity regions were examined over two 12-h periods. Variables characterizing the time of day, conditions of the atmosphere, and distance from the coastline were examined in four sets of Mann–Whitney *U* tests in which cases were grouped according to whether raining areas increased or decreased over a 12-h period. Changes in rain-field size were associated with the diurnal cycle as growth occurred during the late morning and early afternoon after maximum RH and minimum air temperatures had been reached. Rain fields decreased in areal extent in the late-evening hours. TCs completing an ET within 74 h of landfall had the largest rain fields at the time of landfall, and total raining area increased during the first 12 h after landfall but decreased during Per2. Regions of high reflectivity decreased in areal coverage for ET cases save when the diurnal cycle likely contributed to growth in the late morning and early afternoon. Moisture was also important for rain-field

growth. Above the boundary layer, increasing RH in the preceding 12 h was related to rain-field growth as was remaining near the coastline during Per1. In addition, this study found that more TCs made landfall just after midnight as compared with 1950–96 when most landfalls occurred just prior to midnight. This finding is likely due to improvements in observing systems.

This study has provided observational evidence for diurnal variations of raining areas of TCs even as they face rapidly changing environmental conditions while moving over the United States. Associations between environmental conditions and rain-field growth and decay were explored on a broad spatial scale in terms of the environmental variables and on a temporal scale in terms of the radar analysis. The logical next step toward confirming a link between the diurnal cycle and TC rain fields over land through observational data is to examine rain-field evolution at a higher temporal resolution. Further analyses utilizing radar reflectivity data from the WSR-88D network are justified because the precipitation radar swath used to create the TRMM dataset is only 250 km wide. Also, WSR-88D reflectivity data are available every 5–6 min, which is a higher temporal resolution than is available from the TRMM data. The analysis of WSR-88D data over hourly periods will allow the timing of peak rainfall within the diurnal cycle to be more precisely defined along with the rate at which growth and decay occur. Inclusion of level-II reflectivity data in future analysis would allow the vertical development of TC rain fields to be analyzed to aid in the identification of convective regions of the rain fields where the highest rain rates occur. It will also be advantageous to model atmospheric conditions at a higher spatial resolution than the 200–800-km average provided by the SHIPS dataset, particularly in light of the associations between moisture and rain-field growth identified by the current study. It would be appropriate to characterize environmental conditions utilizing NARR data given that they are available every 3 h at a 32-km spatial resolution (Mesinger et al. 2006).

Acknowledgments. This research was supported by a National Science Foundation CAREER Award BCS-1053864. The comments of four anonymous reviewers improved this manuscript.

REFERENCES

Arndt, D. S., J. B. Basara, R. A. McPherson, B. G. Illston, G. D. McManus, and D. B. Demko, 2009: Observations of the overland reintensification of Tropical Storm Erin (2007). *Bull. Amer. Meteor. Soc.,* **90,** 1079–1093.

Atallah, E. H., and L. R. Bosart, 2003: The extratropical transition and precipitation distribution of Hurricane Floyd (1999). *Mon. Wea. Rev.,* **131,** 1063–1081.

Au-Yeung, A. Y. M., and J. C. L. Chan, 2010: The effect of a river delta and coastal roughness variation on a landfalling tropical cyclone. *J. Geophys. Res.,* **115,** D19121, doi:10.1029/2009JD013631.

Barnes, G. M., J. F. Gamache, M. A. Lemone, and G. J. Stossmeister, 1991: A convective cell in a hurricane rainband. *Mon. Wea. Rev.,* **119,** 776–794.

Biggerstaff, M. I., and S. A. Listemaa, 2000: An improved scheme for convective/stratiform echo classification using radar reflectivity. *J. Appl. Meteor.,* **39,** 2129–2150.

Bluestein, H. B., and D. S. Hazen, 1989: Doppler-radar analysis of a tropical cyclone over land: Hurricane Alicia (1983) in Oklahoma. *Mon. Wea. Rev.,* **117,** 2594–2611.

Browner, S. P., W. L. Woodley, and C. G. Griffith, 1977: Diurnal oscillation of the area of cloudiness associated with tropical storms. *Mon. Wea. Rev.,* **105,** 856–864.

Chan, J. C. L., K. S. Liu, S. E. Ching, and E. S. T. Lai, 2004: Asymmetric distribution of convection associated with tropical cyclones making landfall along the south China coast. *Mon. Wea. Rev.,* **132,** 2410–2420.

Cubukcu, N., R. L. Pfeffer, and D. E. Dietrich, 2000: Simulation of the effects of bathymetry and land–sea contrasts on hurricane development using a coupled ocean–atmosphere model. *J. Atmos. Sci.,* **57,** 481–492.

Czajkowski, J., K. Simmons, and D. Sutter, 2011: An analysis of coastal and inland fatalities in landfalling US hurricanes. *Nat. Hazards,* **59,** 1513–1531.

Dai, A., 2001: Global precipitation and thunderstorm frequencies. Part II: Diurnal variations. *J. Climate,* **14,** 1112–1128.

——, X. Lin, and K. L. Hsu, 2007: The frequency, intensity, and diurnal cycle of precipitation in surface and satellite observations over low- and mid-latitudes. *Climate Dyn.,* **29,** 727–744.

DeMaria, M., and J. Kaplan, 1994: A Statistical Hurricane Intensity Prediction Scheme (SHIPS) for the Atlantic basin. *Wea. Forecasting,* **9,** 209–220.

——, M. Mainelli, L. K. Shay, J. A. Knaff, and J. Kaplan, 2005: Further improvements to the Statistical Hurricane Intensity Prediction Scheme (SHIPS). *Wea. Forecasting,* **20,** 531–543.

Emanuel, K., J. Callaghan, and P. Otto, 2008: A hypothesis for the redevelopment of warm-core cyclones over northern Australia. *Mon. Wea. Rev.,* **136,** 3863–3872.

Frank, W. M., 1977: The structure and energetics of the tropical cyclone I. Storm structure. *Mon. Wea. Rev.,* **105,** 1119–1135.

——, and E. A. Ritchie, 1999: Effects of environmental flow upon tropical cyclone structure. *Mon. Wea. Rev.,* **127,** 2044–2061.

Gray, W. M., and R. W. J. Jacobson, 1977: Diurnal variation of deep cumulus convection. *Mon. Wea. Rev.,* **105,** 1171–1188.

Haggard, W. H., T. H. Bilton, and H. L. Crutcher, 1973: Maximum rainfall from tropical cyclone systems which cross the Appalachians. *J. Appl. Meteor.,* **12,** 50–61.

Harr, P. A., and R. L. Elsberry, 2000: Extratropical transition of tropical cyclones over the western North Pacific. Part I: Evolution of structural characteristics during the transition process. *Mon. Wea. Rev.,* **128,** 2613–2633.

Hart, R. E., and J. L. Evans, 2001: A climatology of the extratropical transition of Atlantic tropical cyclones. *J. Climate,* **14,** 546–564.

Hill, K., and G. M. Lackmann, 2009: Influence of environmental humidity on tropical cyclone size. *Mon. Wea. Rev.,* **137,** 3294–3315.

Houze, R. A., 1993: *Cloud Dynamics.* Academic Press, 573 pp.

Jarvinen, B. R., C. J. Neumann, and M. A. S. Davis, 1984: A tropical cyclone data tape for the North Atlantic basin, 1886–1983. NOAA Tech. Memo. NWS NHC 22, 21 pp. [Available online at http://www.nhc.noaa.gov/pdf/NWS-NHC-1988-22.pdf.]

Jiang, H., J. B. Halverson, J. Simpson, and E. J. Zipser, 2008: On the differences in storm rainfall from Hurricanes Isidore and Lili. Part II: Water budget. *Wea. Forecasting,* **23,** 44–61.

——, C. Liu, and E. J. Zipser, 2011: A TRMM-based tropical cyclone cloud and precipitation feature database. *J. Appl. Meteor. Climatol.,* **50,** 1255–1274.

Jones, S. C., and Coauthors, 2003: The extratropical transition of tropical cyclones: Forecast challenges, current understanding, and future directions. *Wea. Forecasting,* **18,** 1052–1092.

Jorgensen, D. P., 1984: Mesoscale and convective-scale characteristics of mature hurricanes. Part I: General observations by research aircraft. *J. Atmos. Sci.,* **41,** 1268–1285.

Kellner, O., D. Niyogi, M. Lei, and A. Kumar, 2012: The role of anomalous soil moisture on the inland reintensification of Tropical Storm Erin (2007). *Nat. Hazards,* **63,** 1573–1600.

Kikuchi, K., and B. Wang, 2008: Diurnal precipitation regimes in the global tropics. *J. Climate,* **21,** 2680–2696.

Kimball, S. K., 2008: Structure and evolution of rainfall in numerically simulated landfalling hurricanes. *Mon. Wea. Rev.,* **136,** 3822–3847.

Klein, P. M., P. A. Harr, and R. L. Elsberry, 2000: Extratropical transition of western North Pacific tropical cyclones: An overview and conceptual model of the transformation stage. *Wea. Forecasting,* **15,** 373–395.

Konrad, C. E., 2001: Diurnal variations in the landfall times of tropical cyclones over the eastern United States. *Mon. Wea. Rev.,* **129,** 2627–2631.

——, M. F. Meaux, and D. A. Meaux, 2002: Relationships between tropical cyclone attributes and precipitation totals: Considerations of scale. *Int. J. Climatol.,* **22,** 237–247.

Kossin, J. P., 2002: Daily hurricane variability inferred from GOES infrared imagery. *Mon. Wea. Rev.,* **130,** 2260–2270.

Lajoie, F. A., and I. J. Butterworth, 1984: Oscillation of high-level cirrus and heavy precipitation around Australian region tropical cyclones. *Mon. Wea. Rev.,* **112,** 535–544.

Liu, K. S., J. C. L. Chan, W. C. Cheng, S. L. Tai, and P. W. Wong, 2007: Distribution of convection associated with tropical cyclones making landfall along the South China coast. *Meteor. Atmos. Phys.,* **97,** 57–68.

Lonfat, M., R. Rogers, T. Marchok, and F. D. Marks, 2007: A parametric model for predicting hurricane rainfall. *Mon. Wea. Rev.,* **135,** 3086–3097.

Mann, H. B., and D. R. Whitney, 1947: On a test of whether one of two random variables is stochastically larger than the other. *Ann. Math. Stat.,* **18,** 50–60.

Matyas, C. J., 2007: Quantifying the shapes of U.S. landfalling tropical cyclone rain shields. *Prof. Geogr.,* **59,** 158–172.

——, 2010: Associations between the size of hurricane rain fields at landfall and their surrounding environments. *Meteor. Atmos. Phys.,* **106,** 135–148.

Maxwell, J. T., P. T. Soule, J. T. Ortegren, and P. A. Knapp, 2012: Drought-busting tropical cyclones in the southeastern Atlantic United States: 1950–2008. *Ann. Assoc. Amer. Geogr.,* **102,** 259–275.

Medlin, J. M., S. K. Kimball, and K. G. Blackwell, 2007: Radar and rain gauge analysis of the extreme rainfall during Hurricane Danny's (1997) landfall. *Mon. Wea. Rev.,* **135,** 1869–1888.

Mesinger, F., and Coauthors, 2006: North American Regional Reanalysis. *Bull. Amer. Meteor. Soc.,* **87,** 343–360.

Muramatsu, T., 1983: Diurnal-variations of satellite-measured TBB areal distribution and eye diameter of mature typhoons. *J. Meteor. Soc. Japan,* **61,** 77–90.

NHC, cited 2012: NHC issuance criteria changes for tropical cyclone watches/warnings. [Available online at http://www.nhc.noaa.gov/watchwarn_changes.shtml.]

Office of the Federal Coordinator for Meteorological Services and Supporting Research (OFCM), 2006: Federal meteorological handbook 11: Doppler radar meteorological observations—Part D, WSR-88D Unit Description and Operational Applications. FCM-H11D-2006, 218 pp. [Available online at http://www.ofcm.gov/fmh11/fmh11partd/pdf/FMH11D-2006.pdf.]

Parrish, J. R., R. W. Burpee, F. D. Marks, and R. Grebe, 1982: Rainfall patterns observed by digitized radar during the landfall of Hurricane Frederic (1979). *Mon. Wea. Rev.,* **110,** 1933–1944.

Rappaport, E. N., 2000: Loss of life in the United States associated with recent Atlantic tropical cyclones. *Bull. Amer. Meteor. Soc.,* **81,** 2065–2073.

——, and Coauthors, 2009: Advances and challenges at the National Hurricane Center. *Wea. Forecasting,* **24,** 395–419.

Ritchie, E. A., and R. L. Elsberry, 2001: Simulations of the transformation stage of the extratropical transition of tropical cyclones. *Mon. Wea. Rev.,* **129,** 1462–1480.

Rodgers, E. B., S. W. Chang, J. Stout, J. Steranka, and J. J. Shi, 1991: Satellite-observations of variations in tropical cyclone convection caused by upper-tropospheric troughs. *J. Appl. Meteor.,* **30,** 1163–1184.

Rogers, R. F., and R. E. Davis, 1993: The effect of coastline curvature on the weakening of Atlantic tropical cyclones. *Int. J. Climatol.,* **13,** 287–299.

Sheets, R. C., 1990: The National Hurricane Center—Past, present, and future. *Wea. Forecasting,* **5,** 185–232.

Steiner, M., R. A. Houze, and S. E. Yuter, 1995: Climatological characterization of three-dimensional storm structure from operational radar and rain-gauge data. *J. Appl. Meteor.,* **34,** 1978–2007.

Steranka, J., E. B. Rodgers, and R. C. Gentry, 1984: The diurnal variation of Atlantic Ocean tropical cyclone cloud distribution inferred from geostationary satellite infrared measurements. *Mon. Wea. Rev.,* **112,** 2338–2344.

Sturdevant-Rees, P., J. A. Smith, J. Morrison, and M. L. Baeck, 2001: Tropical storms and the flood hydrology of the central Appalachians. *Water Resour. Res.,* **37,** 2143–2168.

Tokay, A., and D. A. Short, 1996: Evidence from tropical raindrop spectra of the origin of rain from stratiform versus convective clouds. *J. Appl. Meteor.,* **35,** 355–371.

Tuleya, R. E., 1994: Tropical storm development and decay: Sensitivity to surface boundary conditions. *Mon. Wea. Rev.,* **122,** 291–304.

Vincent, D. G., and A. H. Fink, 2001: Tropical cyclone environments over the northeastern and northwestern Pacific based on ERA-15 analyses. *Mon. Wea. Rev.,* **129,** 1928–1948.

Wallace, J. M., 1975: Diurnal variations in precipitation and thunderstorm frequency over the conterminous United States. *Mon. Wea. Rev.,* **103,** 406–419.

Wilks, D. S., 1995: *Statistical Methods in the Atmospheric Sciences: An Introduction.* Academic Press, 467 pp.

Yang, S., and E. A. Smith, 2006: Mechanisms for diurnal variability of global tropical rainfall observed from TRMM. *J. Climate,* **19,** 5190–5226.

Yokoyama, C., and Y. N. Takayabu, 2008: A statistical study on rain characteristics of tropical cyclones using TRMM satellite data. *Mon. Wea. Rev.,* **136,** 3848–3862.